Supporting Information

Efficient Direct Lignin Fuel Cell Enabled by Hierarchical Nickel-Iron Phosphide Nanosheets as Anode Catalyst†

Fei Liu,‡[a] A Lusi,‡[b] Harish Radhakrishnan,[b] Hengzhou Liu,[c] Wenzhen Li,[c] Hantang Qin,[d] Shan Jiang,[a] Xianglan Bai,[b] and Hu Shan*[b]

a Department of Materials Science and Engineering, Iowa State University, Ames, IA, 50011, United States.
b Department of Mechanical Engineering, Iowa State University, Ames, IA, 50011, United States.
c Department of Chemical and Biological Engineering, Iowa State University, Ames, IA, 50011, United States.
d Department of Industrial and Manufacturing Systems Engineering, Iowa State University, Ames, IA, 50011, United States.

‡ These authors contribute equally.

*Email: shanhu@iastate.edu

Table S1. Ultimate analysis, proximate, and molecular weight distributions of lignin samples.

	ADM lignin	SKL lignin
N [%]	1.64	0.67
C [%]	60.34	61.79
H [%]	4.65	4.94
S [%]	0.28	1.61
O [%]	33.09	30.99
Moisture [wt%]	3.9	2.3
Volatile [wt%]	61.1	55.1
Fixed Carbon [wt%]	27.2	38.8
Ash [wt%]	5.9	2.6
Number Average M_n [Da]	1296	1215
Weight Average M_w [Da]	6330	5505
Polydispersity PD	4.89	4.53

Table S2. ICP-OES data for NiFeP catalysts.

Ni/Fe content in the precursor solution		Ni/Fe content in the catalyst	
Ni (%)	Fe (%)	Ni (%)	Fe (%)

90%	10%	91.2%	8.8%
70%	30%	71.9%	28.1%
50%	50%	51.2%	48.8%

Table S3. A comparison of different fuel cells using lignin or lignocellulosic biomass as feedstock.

Fuel Cell Type	Fuels	Anode catalyst	Heterogeneous or Homogeneous catalysts	Power density (mW cm^{-2})	Ref.
MFC	Rice straw	Bacteria	-	0.0145	[1]
MFC	Rice straw	Bacteria	-	0.019	[2]
MFC	Corn stover	Bacteria	-	0.0331	[3]
AFC	Barley straw	Methyl viologen	Homogeneous	0.04	[4]
LFFC	Wheat straw	$H_3PMo_{12}O_{40}$ $H_4PMo_{11}VO_{40}$	Homogeneous	10.8 12.4	[5]
LFFC	Wheat straw	$H_3PMo_{12}O_{40}$	Homogeneous	11	[6]
LFFC	Corn stover Corn cob Peanut shell	$H_3PMo_{12}O_{40}$	Homogeneous	28 - 35	[7]
LFFC	Wheat straw	Methylene blue	Homogeneous	12.3 (acid) 41.8 (alkaline)	[8]
LFFC	Kraft lignin	$H_3PMo_{12}O_{40}$	Homogeneous	5	[9]
LFFC	Corn stover alkaline lignin	$K_3Fe(CN)_6$	Homogeneous	200	[10]
LFFC	kraft black liquor and spent sulfite liquor	Pt, Ni	Heterogeneous	1.4	[11]
LFFC	Lignin–sulfonic acid	TiO_2/Co TiO_2/Cu TiO_2/Ni TiO_2/Os	Heterogeneous	0.061	[12]
LFFC	Corn stover lignin	NiFeP	Heterogeneous	24	This work

Table S4. FTIR peaks and corresponding functional groups of ADM lignin before and after fuel cell reaction.

Wavenumber [cm^{-1}]	Structure and functional group
3362	Hydroxyl group in phenolic and aliphatic structures

2945	CH stretching in aromatic methoxy groups and methylene group side chains
2917, 2848, 2833	CH stretching in aliphatic methylene group
1718, 1707	Unconjugated Carbonyl/carboxyl stretching
1689	Conjugated carbonyl/carboxyl stretching
1605, 1515, 1424	Aromatic skeletal vibrations
1462	C-H deformation combined with aromatic ring vibration
1376	Phenolic OH and aliphatic C-H in methyl groups
1329	Syringyl (S) ring and guaiacyl (G) ring condensed
1272	G ring and C=O stretching
1220	Stretching of C-C, C-O and C=O
1140	C-H in-plane deformation of G units
1120	C-H in-plane deformation of S units
1084, 1031	C-O deformation in alcohols and aliphatic ethers, and the unconjugated C=O stretch
1035	Aromatic C-H deformation
854, 817	C-H out-of-plane vibrations in position 2, 5 and 6 of G units
832	H units in corn stover; C-H out-of-plane vibration in position 2 and 6 of S units

*Peaks are identified based on the previous studies.[13-15]

Table S5. Proximate analysis of acid washed ADM lignin.

	Acid washed ADM lignin
Moisture [wt%]	**2.9**
Volatile [wt%]	**60.6**
Fixed Carbon [wt%]	**33.4**
Ash [wt%]	**3.0**

Table S6. ICP-OES results of ADM lignin and acid washed ADM lignin.

	ADM lignin	**Acid washed ADM lignin**
Al [ppm]	1314	1244

Ca [ppm]	1918	211
Cu [ppm]	2	-24
Fe [ppm]	1043	785
Mg [ppm]	601	223
Mn [ppm]	80	45
P [ppm]	492	93
Zn [ppm]	-55	-73
Na [ppm]	1603	1458
K [ppm]	4086	262

Table S7. Molecular weight distribution of acid washed ADM lignin.

	Acid washed ADM lignin
Number Average Mn [Da]	1381
Weight Average Mw [Da]	6482
Polydispersity PD	4.70

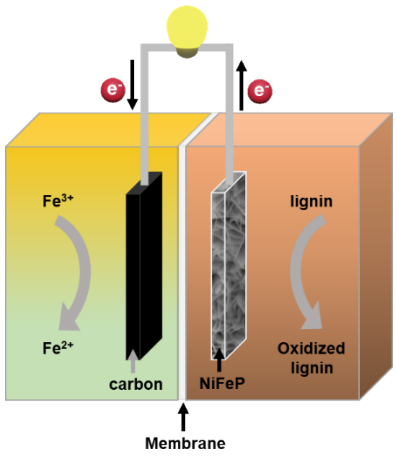

Figure S1. Schematic diagram of the direct lignin fuel cell.

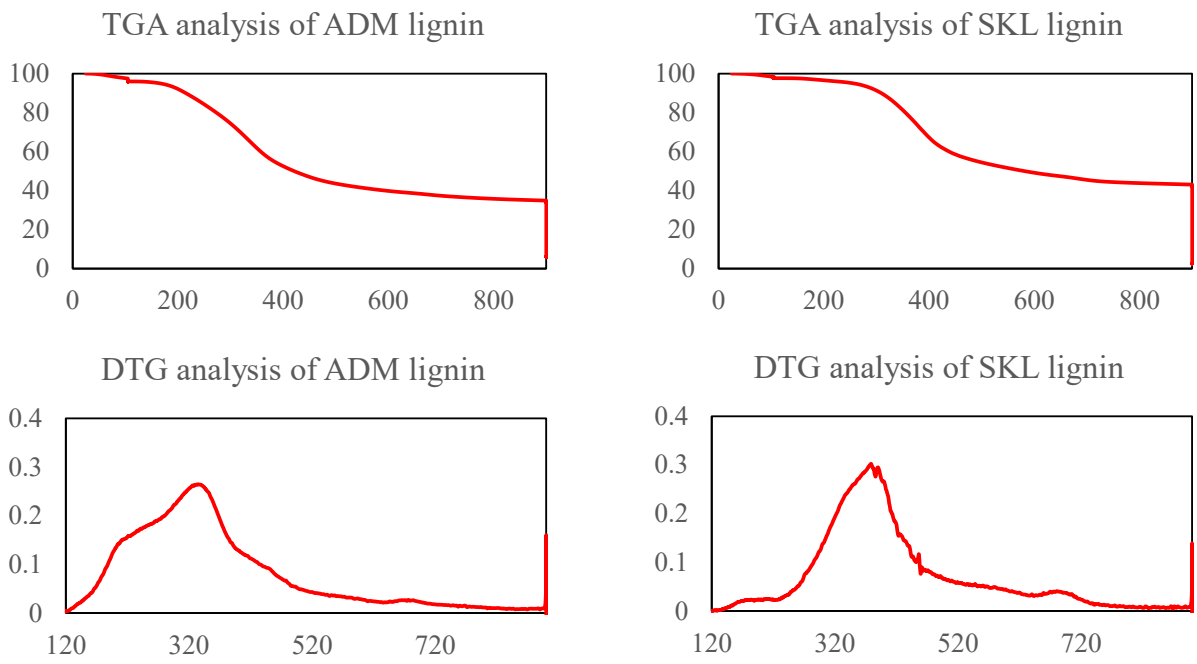

Figure S2. TGA/DTG analysis of lignin samples.

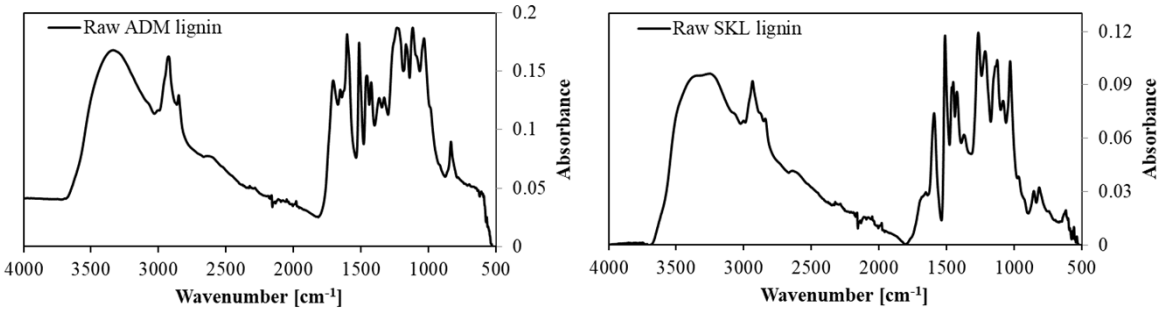

Figure S3. Fourier transform infrared spectroscopy (FTIR) analysis of lignin samples.

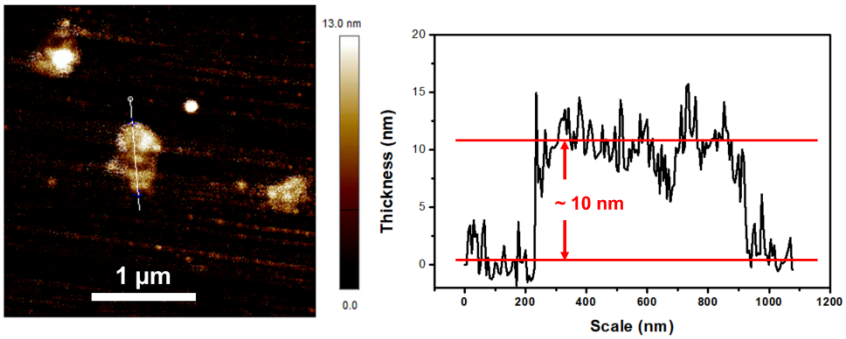

Figure S4. An atomic force microscopy image of NiFeP nanosheets and corresponding height profile of a typical nanosheet.

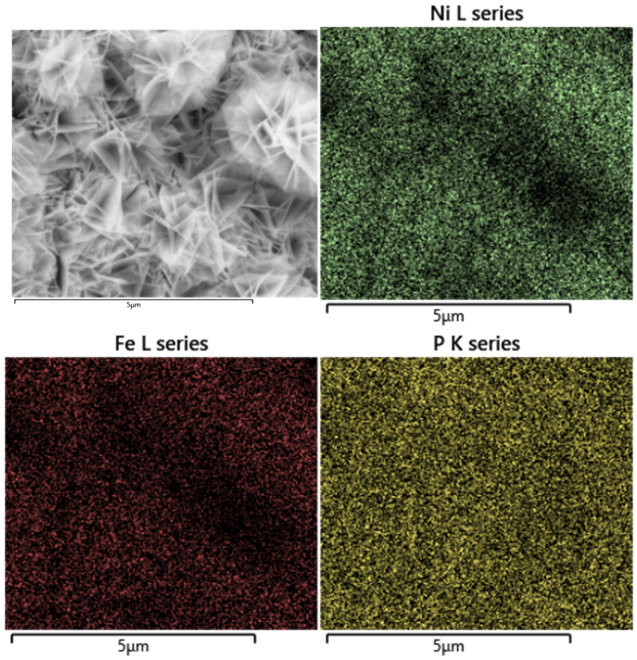

Figure S5. SEM and EDS elemental mapping images of NiFeP.

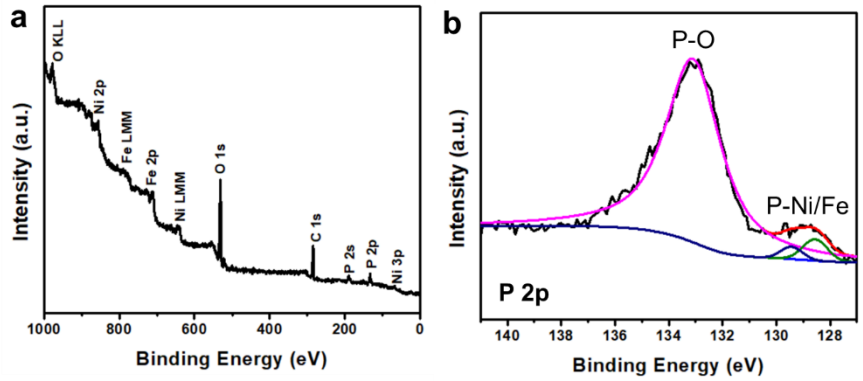

Figure S6. (a) XPS survey spectrum and (b) P 2p spectrum of NiFeP.

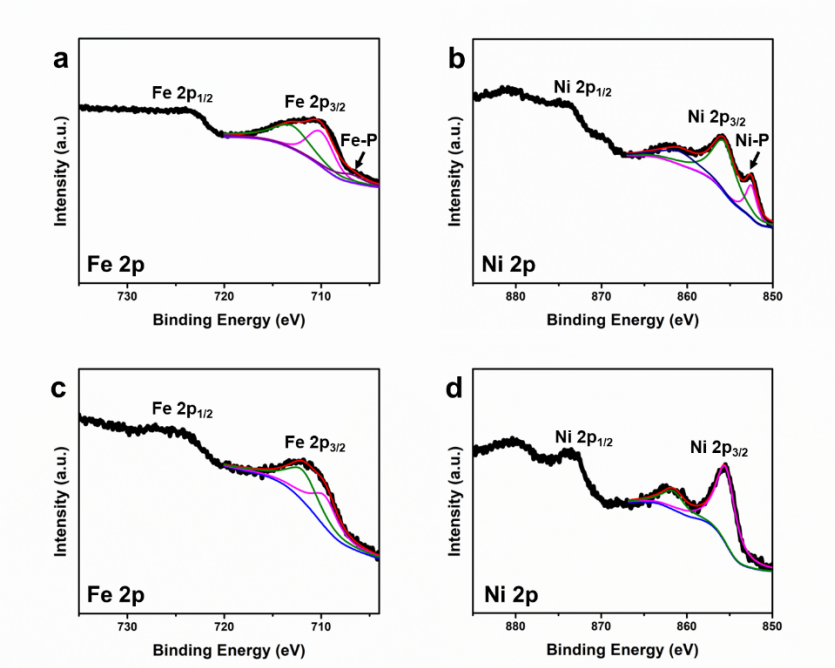

Figure S7. Fe and Ni 2p spectra of NiFeP (a, b) before and (c, d) after fuel cell process.

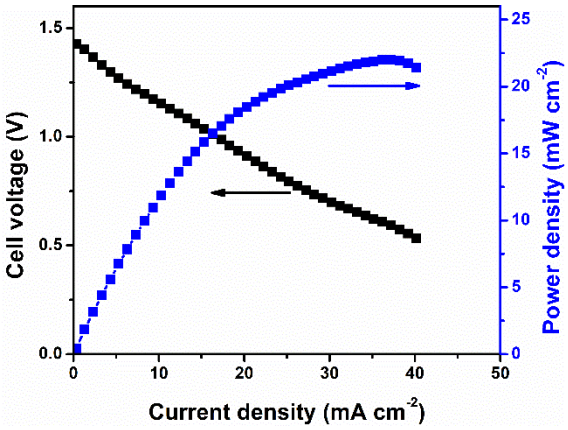

Figure S8. Polarization and power curves of the fuel cell using NiFeP on carbon cloth as the anode catalyst.

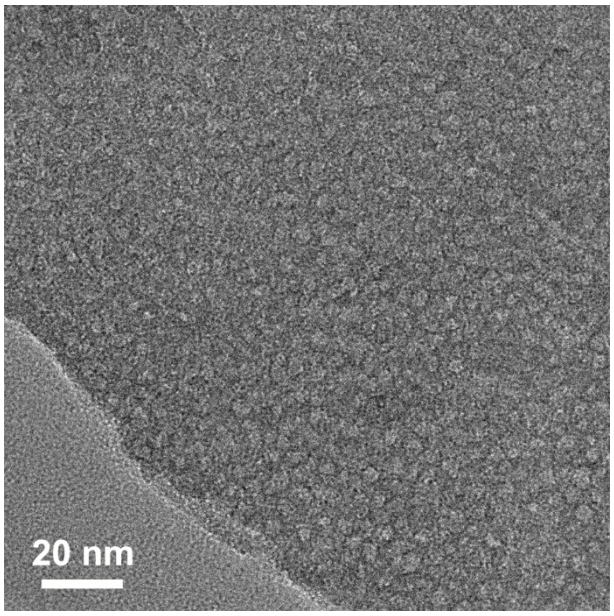

Figure S9. TEM image of NiFeP nanosheets showing abundant mesopores on the nanosheet surface.

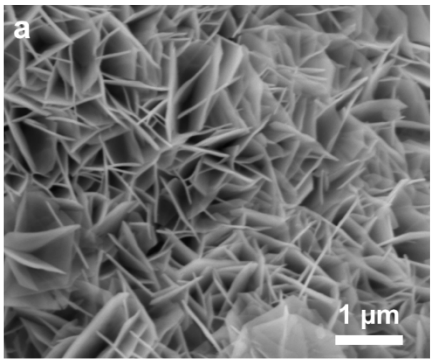

b

	Before fuel cell reaction (at. %)	After fuel cell reaction (at. %)
C	4.17	46.38
O	49.02	34.95
P	12.35	1.07
Fe	12.39	4.33
Ni	22.08	10.03
Al		1.56
K		1.68

Figure S10. (a) SEM image of NiFeP nanosheets after fuel cell process. (b) Elemental composition of NiFeP nanosheets before and after fuel cell process determined by EDS.

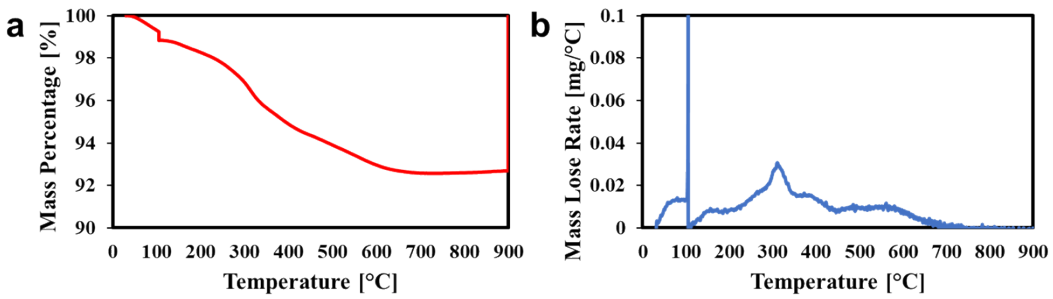

Figure S11. (a) TGA and (b) DTG analyses of NiFeP nanosheets after fuel cell process.

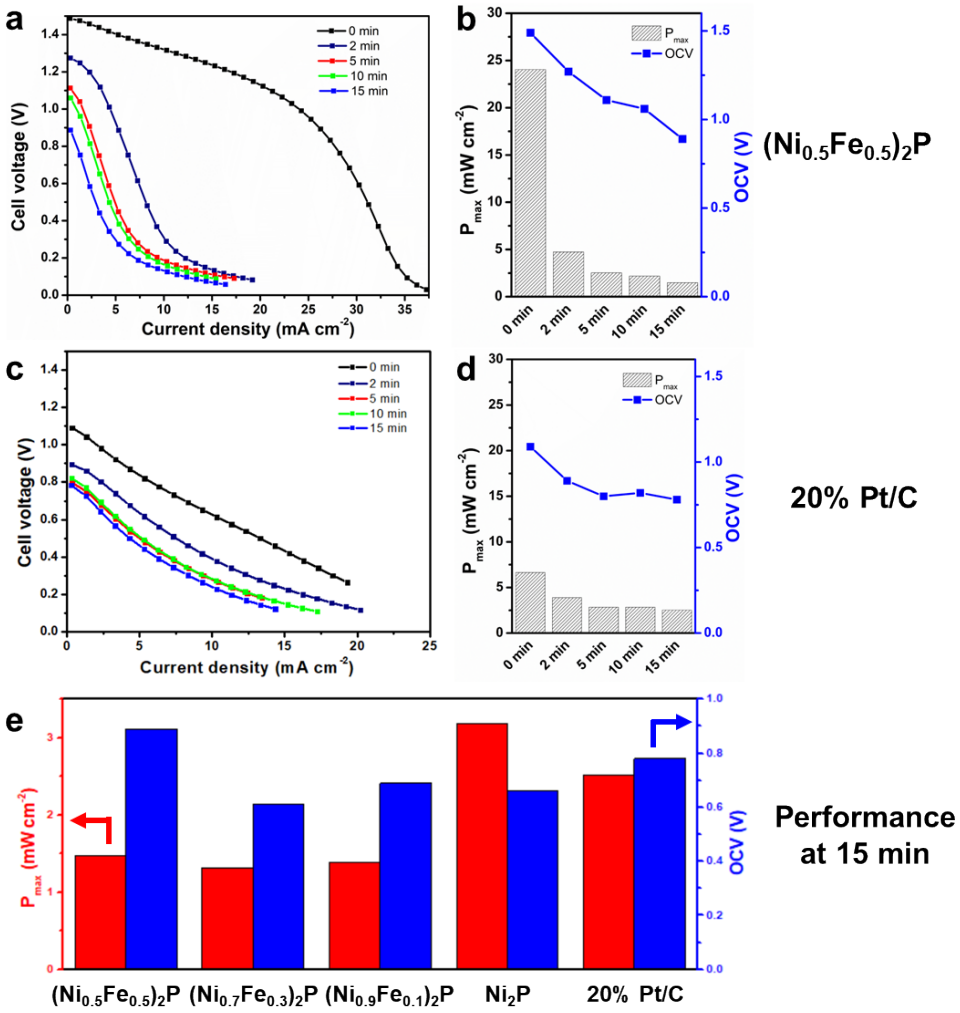

Figure S12. (a) Polarization curve, (b) P_{max} and OCV of the fuel cell as a function of operation time using $(Ni_{0.5}Fe_{0.5})_2P$ as the anode catalyst. (c) Polarization curve, (d) P_{max} and OCV of the fuel cell as a function of operation time using Pt/C as the anode catalyst. (e) P_{max} and OCV of the fuel cell at the operation time of 15 min using different anode catalyst.

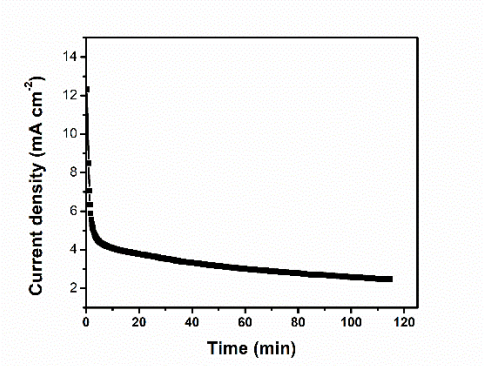

Figure S13. Constant voltage discharging at 0.2 V.

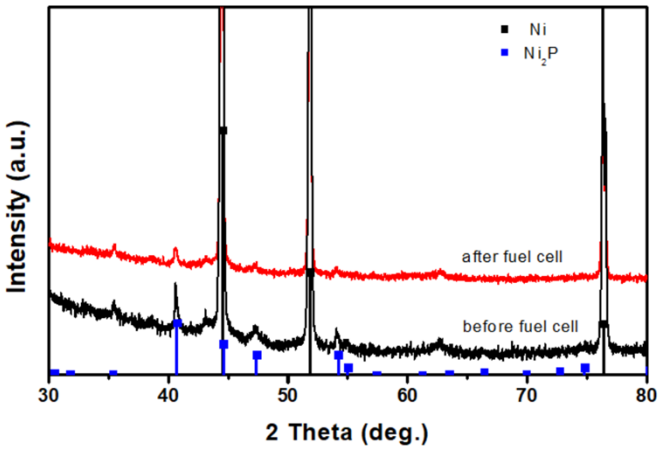

Figure S14. XRD patterns of NiFeP before and after fuel cell process.

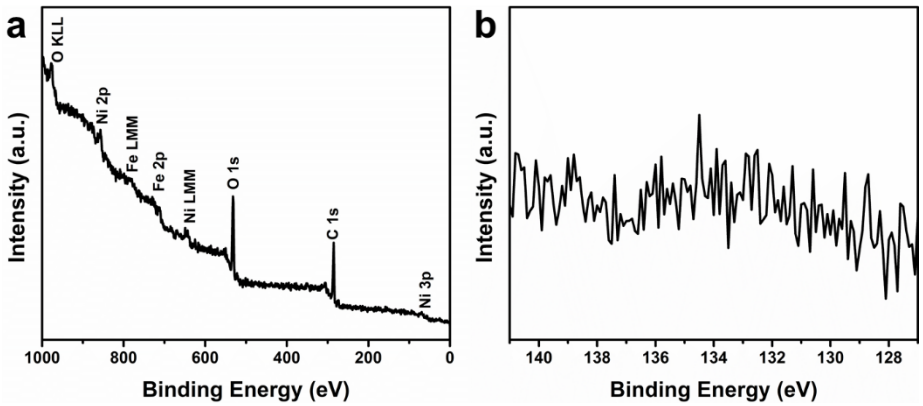

Figure S15. (a) XPS survey spectrum and (b) P 2p spectrum of NiFeP after fuel cell process.

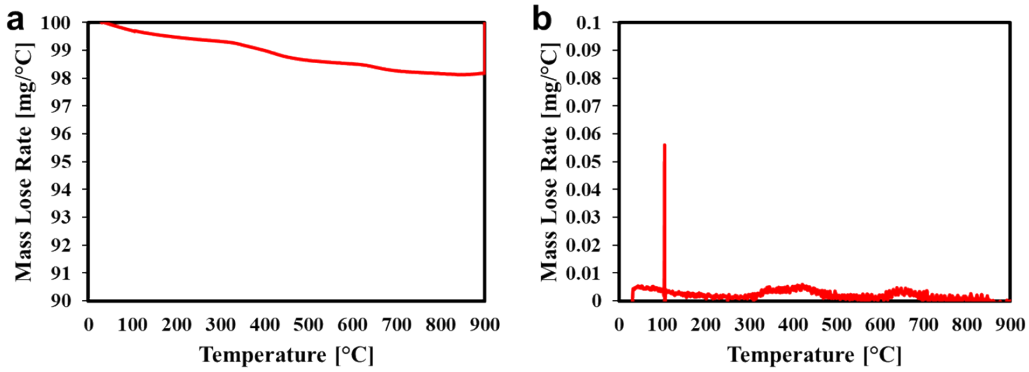

Figure S16. (a) TGA and (b) DTG analyses of the catalyst after reactivation.

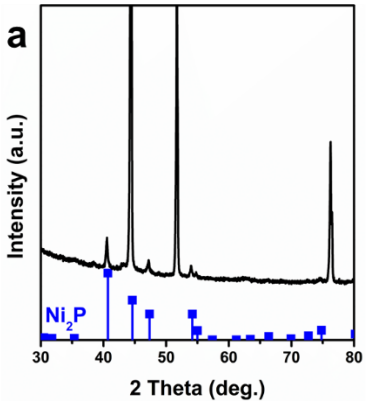

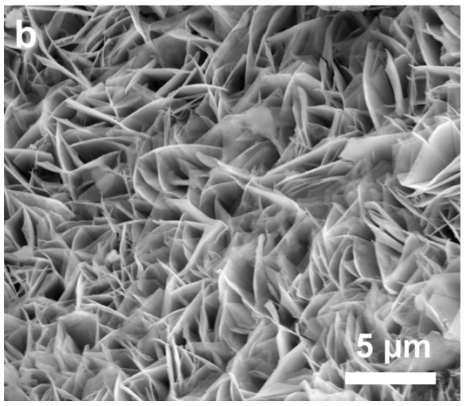

c

Element	Atomic ratio
C	2.1
O	54.1
P	13.62
Fe	9.8
Ni	14.94
K	3.81

Figure S17. (a) XRD pattern, (b) SEM image and (c) EDS elemental composition of the catalyst after reactivation.

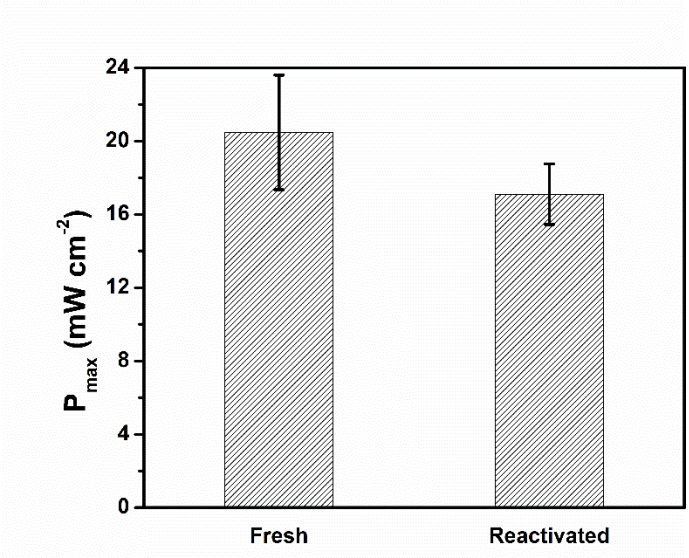

Figure S18. Maximum power density of the fuel cell using fresh and reactivated NiFeP catalyst. Error bars indicate the standard deviations of three replicates.

References:

1. Hassan, S. H. A.; Gad El-Rab, S. M. F.; Rahimnejad, M.; Ghasemi, M.; Joo, J.-H.; Sik-Ok, Y.; Kim, I. S.; Oh, S.-E., Electricity generation from rice straw using a microbial fuel cell. *Int. J. Hydrogen Energy* **2014,** *39* (17), 9490-9496.

2. Gurung, A.; Oh, S. E., Rice Straw as a Potential Biomass for Generation of Bioelectrical Energy Using Microbial Fuel Cells (MFCs). *Energy Sources Part A-Recovery Util. Environ. Eff.* **2015,** *37* (24), 2625-2631.

3. Wang, X.; Feng, Y.; Wang, H.; Qu, Y.; Yu, Y.; Ren, N.; Li, N.; Wang, E.; Lee, H.; Logan, B. E., Bioaugmentation for Electricity Generation from Corn Stover Biomass Using Microbial Fuel Cells. *Environ. Sci. Technol.* **2009,** *43* (15), 6088-6093.
4. Li, S.; Song, X., Study on the preparation and production factors of a direct lignocellulose biomass fuel cell. *J. Electroanal. Chem.* **2018,** *810*, 55-61.
5. Zhao, X.; Ding, Y.; Du, B.; Zhu, J. Y.; Liu, D., Polyoxometalate-Mediated Lignin Oxidation for Efficient Enzymatic Production of Sugars and Generation of Electricity from Lignocellulosic Biomass. *Energy Technol.* **2017,** *5* (8), 1179-1185.
6. Ding, Y.; Du, B.; Zhao, X.; Zhu, J. Y.; Liu, D., Phosphomolybdic acid and ferric iron as efficient electron mediators for coupling biomass pretreatment to produce bioethanol and electricity generation from wheat straw. *Bioresour. Technol.* **2017,** *228*, 279-289.
7. Liu, W.; Gong, Y.; Tricker, A.; Wu, G.; Liu, C.; Chao, Z.-s.; Deng, Y., Fundamental Study toward Improving the Performance of a High-Moisture Biomass-Fueled Redox Flow Fuel Cell. *Ind. Eng. Chem. Res.* **2020,** *59* (10), 4817-4828.
8. Chen, Y. A.; Yang, H. S.; Ouyang, D. H.; Liu, T. X.; Liu, D. H.; Zhao, X. B., Construction of electron transfer chains with methylene blue and ferric ions for direct conversion of lignocellulosic biomass to electricity in a wide pH range. *Appl. Catal. B-Environ.* **2020,** *265*.
9. Zhao, X. B.; Zhu, J. Y., Efficient Conversion of Lignin to Electricity Using a Novel Direct Biomass Fuel Cell Mediated by Polyoxometalates at Low Temperatures. *ChemSusChem* **2016,** *9* (2), 197-207.
10. Ouyang, D.; Wang, F.; Hong, J.; Gao, D.; Zhao, X., Ferricyanide and vanadyl (V) mediated electron transfer for converting lignin to electricity by liquid flow fuel cell with power density reaching 200 mW/cm2. *Appl. Energy* **2021,** *304*, 117927.
11. Oliveira, R. C. P.; Jeremias, M. J.; Mateus, M. M.; Santos, D. M. F., Developing a novel direct liquid fuel cell based on pulping liquors. *Fuel Cells* **2022,** *22* (1-2), 39-47.
12. Kaneko, M.; Ueno, H., Direct biomass fuel cell (BMFC) for polymeric biomass with anode/catalyst device comprising a mesoporous n-semiconductor film/Co, Ni or Cu thin layer. *Electrochim. Acta* **2013,** *90*, 682-689.
13. Faix, O. Fourier transform infrared spectroscopy. *Methods in lignin chemistry*. Springer, Berlin, Heidelberg, 1992. 83-109.
14. C. G. Boeriu, D. Bravo, R. J. A. Gosselink and J. E. G. van Dam, *Ind. Crop. Prod.*, 2004, **20**, 205-218.
15. S. Zhou, Y. Xue, A. Sharma and X. Bai, *ACS Sustainable Chemistry & Engineering*, 2016, **4**, 6608-6617.